CHEMISTRY
A EUROPEAN JOURNAL

DOI: 10.1002/chem.200500834

A Mechanistic and Kinetic Study of the Formation of Metal Nanoparticles by Using Synthetic Tyrosine-Based Oligopeptides

Satyabrata Si,[a] Rama Ranjan Bhattacharjee,[a] Arindam Banerjee,[b] and Tarun K. Mandal*[a]

Abstract: Synthetic oligopeptides containing redox-active tyrosine residues have been employed to prepare gold and silver nanoparticles. In this reduction process an electron from the tyrosinate ion of the peptide is transferred to the metal ion at basic pH through the formation of a tyrosyl radical, which is eventually converted to its dityrosine form during the reaction. This reaction mechanism was confirmed from UV-visible, fluorescence, and EPR spectroscopy and was found to be pH-dependent. Transmission electron microscopy measurement shows that the average size and the monodispersity of gold nanoparticles increase as the number of tyrosine residues in the peptide increases. The kinetic study, based on spectrophotometric measurements of the surface plasmon resonance optical property, shows that the rate of formation of gold nanoparticles was much faster at higher pH than at lower pH and was also dependent on the number of tyrosine residues present in the peptide. The dityrosine form of the peptide was found to retain reducing properties like those of tyrosine in basic medium.

Keywords: dityrosine · gold · kinetics · nanostructures · oligopeptides · radicals

Introduction

Nowadays, metal nanoparticles are attracting much attention from chemists, biologists, and materials scientists because of their unusual optoelectronic and chemical properties,[1] which have potential applications in nanoelectronics,[2] bio-analytical processes,[3] and catalysis.[4] Among these, gold nanoparticles (GNPs) are interesting due to their unique size-dependent optical, electronic, and chemical properties. In particular, special emphasis has been given to the synthesis of GNPs immobilized in biomolecules because of their wide range of applications in modern biotechnology as well as in biorecognition-based self-assembly of functionalized nanoparticles.[5–8] These GNPs are generally prepared by $NaBH_4$- or citrate-reduction of $HAuCl_4$ in the presence of a stabilizer (e.g., small organic molecules, polymers, and biomacromolecules) containing at least one $-NH_2$ or $-SH$ group.[4,7] But the presence of the by-product of these reducing agents may create complications when used in some bioanalytical applications. Therefore, it is preferable to use an in situ reduction technique so that the by-product of the system remains compatible with biosystems. Recently, Zhou and co-workers prepared gold–silk fibroin core-shell nanoparticles by using silk fibroin containing tyrosine residues as both reducing and stabilizing agents, but they did not report the detailed nanoparticle formation mechanism.[9] Sastry et al. reported silver ion reduction with tyrosine at high pH, which in turn converted to a semiquinone structure.[10] In our previous work we have reported the formation of GNPs and their self-assembly using a tyrosine-containing short peptide.[11] To the best of our knowledge, nobody has reported the role of tyrosine in the formation of metal nanoparticles in detail. It has been reported that tyrosine has an important function in electron transfer in the photosystem II (PSII), a vital process in nature leading to a neutral tyrosyl

[a] S. Si, R. R. Bhattacharjee, Dr. T. K. Mandal
Polymer Science Unit
Indian Association for the Cultivation of Science
Jadavpur, Kolkata 700 032 (India)
Fax: (+91) 33-2473-2805
E-mail: psutkm@mahendra.iacs.res.in

[b] Dr. A. Banerjee
Department of Biological Chemistry
Indian Association for the Cultivation of Science
Jadavpur, Kolkata 700 032 (India)

Supporting information for this article is available on the WWW under http://www.chemeurj.org/ or from the author: Particle size histogram analysis of gold nanoparticles, silver nanoparticles, NMR spectra of peptide-1, fluorescence spectra of dityrosine, fluorescence study of ligand exchange reaction, mass spectra of peptide-1 in the presence of $Cu(NO_3)_2$, and UV/Vis spectra to study the fate of the tyrosine moiety.

radical.[12–17] Tyrosine also acts as an electron-transfer agent in many enzymes, such as prostaglandin H synthase,[18] galactose oxidase,[19] and ribonucleotide reductase.[20] Here, we report for the first time the mechanism and kinetics of GNP formation through the electron transfer from tyrosine residues present in the oligopeptides to the respective metal ion and also on the fate of the peptide after the reduction process.

Results and Discussion

The detailed synthesis of GNPs using peptide-1 (NH_2-Leu-Aib-Tyr-OMe) at pH ~11 was reported in our previous work.[11] The formation of the GNPs at pH ~9 and ~11 were monitored by using a UV/Vis spectrophotometer to follow the appearance of the surface plasmon (SP) band at 535 and 527 nm, respectively (see Figure 1a and b), characteristic of GNPs within the size range of 20 nm.[21] Two other peptides, containing two (peptide-2, NH_2-Tyr-Aib-Tyr-OMe) and three (peptide-3, NH_2-Tyr-Tyr-Tyr-OMe) tyrosine residues were also employed to study the kinetics of formation of colloidal GNPs. UV/Vis spectra of GNPs prepared with peptide-2 and peptide-3 at pH ~11 (see Figure 1c and d respectively) also exhibit the SP band nearly at the same position as for peptide-1, along with a new peak at about 325 nm. The appearance of the peak at 325 nm will be explained later in this section. TEM images of GNPs prepared at different pH values by using various peptides reveal spherical particles (Figure 2a–d). The particle-size analysis shows that the average diameter of the GNPs at pH ~9 and ~11 are 11.6 ± 2 and 8.7 ± 2.3 nm, respectively (see Figures S1a and b in the Supporting Information for histogram analysis). These data reveal that the distribution of particle size is almost the same for the GNPs prepared at both pH values, but the average particle-size increases at lower pH compared to that prepared at higher pH. The average particle-size of the GNPs was found to be 9.7 ± 1.7 and 15.2 ± 1.4 nm as estimated from the statistical analyses of the GNPs prepared by peptide-2 and peptide-3 respectively (see Figures S1c and d in the Supporting Information for histogram analysis). This clearly indicates that the average particle-size increases with increasing number of tyrosine residues in the peptide. However, the standard deviation value decreases indicating that the monodispersity of the particles increases. This may be the result of better stability of the GNPs by a higher number of tyrosine residues within the peptide molecule.

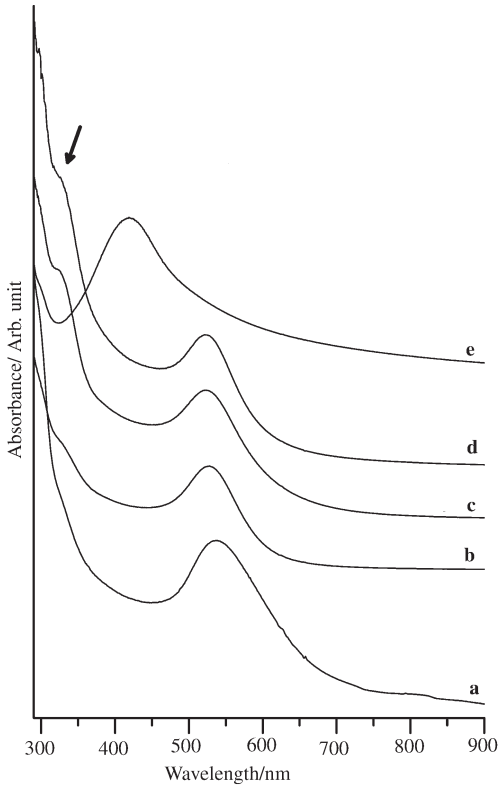

Figure 1. UV/Vis absorbance spectra of suspensions of: a) gold-peptide-1 nanoconjugates at low pH; b) gold-peptide-1 nanoconjugates at high pH; c) gold-peptide-2 nanoconjugates; d) gold-peptide-3 nanoconjugates; and e) silver-peptide-1 nanoconjugates.

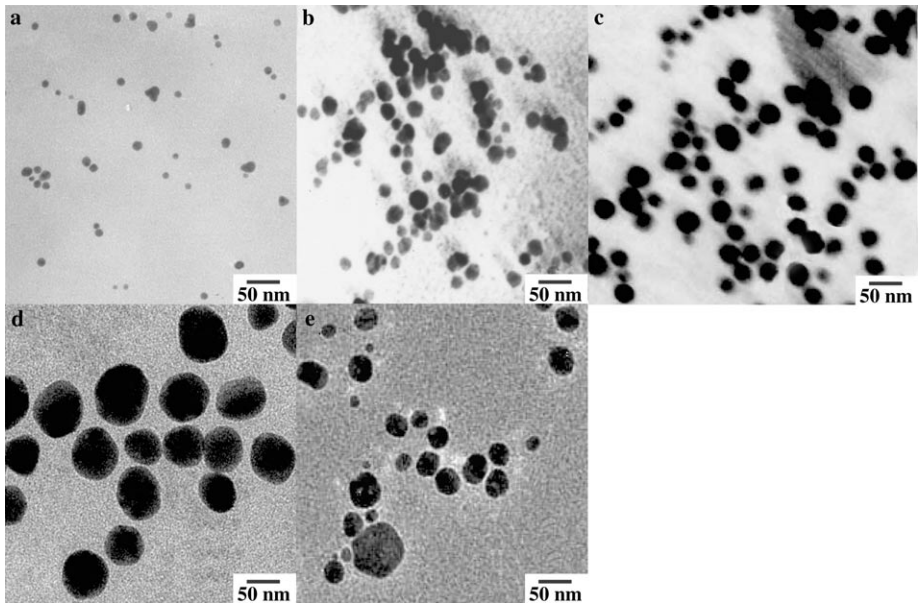

Figure 2. TEM images of gold nanoparticles prepared at: a) pH 11 with peptide-1; b) pH 9 with peptide-1; c) pH 11 with peptide-2; d) pH 11 with peptide-3; and e) silver nanoparticles reduced with peptide-1 at pH 11.

GNPs are most likely stabilized through the interaction of amino groups of peptides with the gold surface as mentioned in our previous work.[11] The gold nanoparticles formed are quite stable for more than six months. The centrifuged and redispersed GNPs also form a stable suspension in water. The hydrolysis of the methoxy group of peptides under our experimental conditions increases the solubility of peptides that might add extra stability to the gold-peptide nanoconjugates when redispersed in water. This has been proved indirectly by performing the same reaction in the absence of gold but maintaining the same pH. The absence of a methoxy proton peak in the NMR spectra of the final extracted peptide from solution reveals the hydrolysis of the methoxy group (see Figure S2b in the Supporting Information). The resultant gold-peptide nanoconjugates were aggregated at pH < 4, further confirming the presence of surface −COOH groups that interact through hydrogen bonding as reported earlier.[22] The ^{1}H NMR spectra of the gold-peptide nanoconjugate in D_2O (see Figure S2c in the Supporting Information) shows the peak for the tyrosine moiety as well as other residues present in the peptide, but the spectra is not so clear (due to the surface-bound peptide) and hence the exact configuration of the peptide could not be predicted.

The UV/Vis spectra of the alkaline peptide-1 solution exhibits an absorbance peak at 292 nm due to the tyrosinate ion, which was shifted to lower wavelengths during the reduction of the gold salt to metallic gold as mentioned in our earlier report.[11] This observation indicates that the tyrosine residue plays some role in this reduction process. We believe that the electron transfer from the tyrosine residues to the gold salt leads to the formation of metallic gold nanoparticles.

To explore this in more detail, the absorbance peak at 292 nm due to the tyrosinate ion was monitored with time during the GNP-formation (see Figure 3). Figure 3 indicates that, as the reaction proceeds, the peak at 292 nm decreases gradually and is shifted towards lower wavelength. This result agrees well with the literature report.[9] But in the case of peptide-3, we cannot distinguish a change of peak position of the tyrosinate ion due to the presence of a higher concentration of tyrosine residues in peptide-3 (Figure 3c). In addition a new peak appeared at about 325 nm (marked by an arrow in Figures 1, 3b, and 3c), which became more prominent in the reduction of the metal ion with peptide-2 and peptide-3 containing a higher number of tyrosine residues compared to peptide-1. The development of this peak at about 325 nm may imply some modification of the tyrosine residues present in the peptide backbone.

To verify that a similar type of reaction is occurring for other metal ions, the same peptide was allowed to react with the Ag^+ ion in alkaline medium at pH ~ 11. This process resulted in the formation of silver nanoparticles, which is evident from their characteristic SP band that appeared at 416 nm as shown in Figure 1e. Figure 2e shows the TEM image of the silver nanoparticles with an average diameter of 13.1 ± 2.9 nm as estimated from TEM analysis (see Figure S1e in the Supporting Information for histogram analysis).

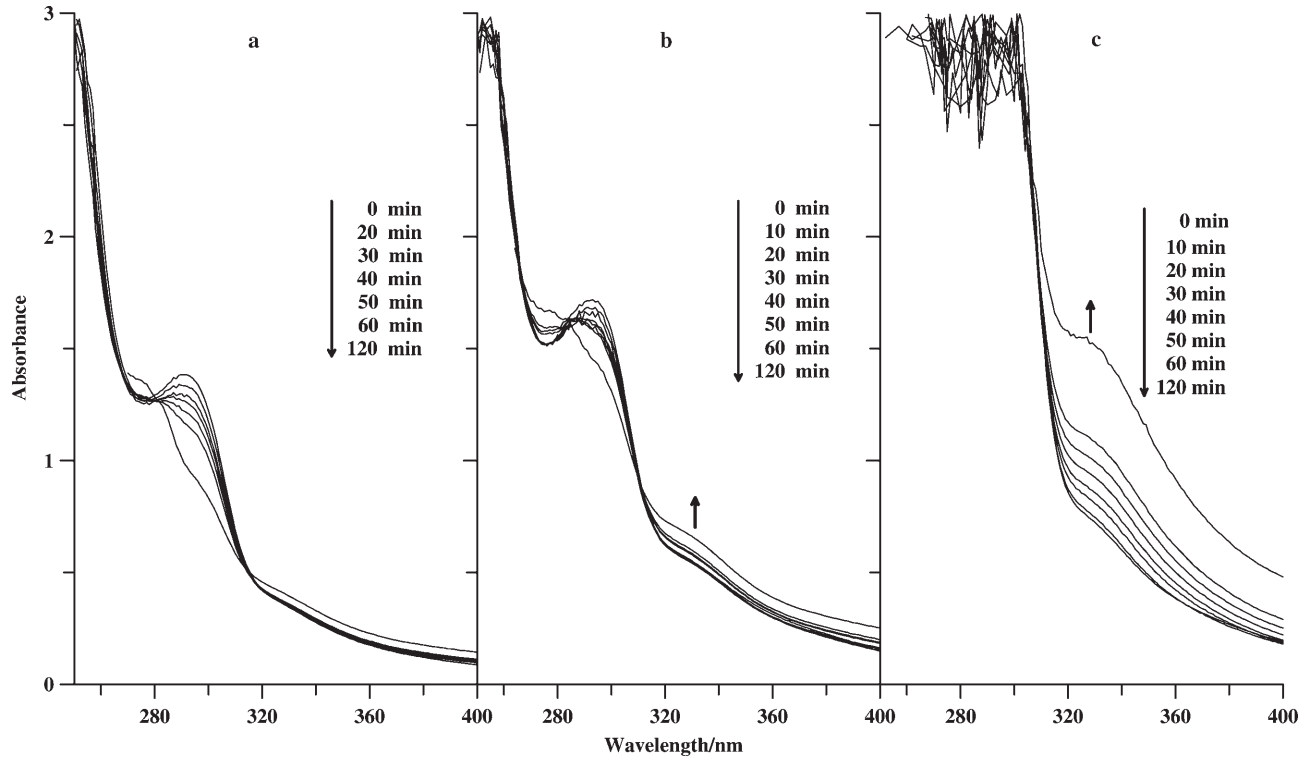

Figure 3. Time-dependent UV/Vis spectral study of tyrosine/tyrosinate in peptides during GNP formation at pH 11 by using: a) peptide-1; b) peptide-2; and c) peptide-3. A new peak developed at 325 nm (marked by an arrow).

This result indicates that the same electron-transfer process occurs and reduces Ag^{I} to metallic Ag^{0}. Formation of metal (gold and silver) nanoparticles was not observed when the reaction was performed with the same peptide in organic medium (such as methanol and tetrahydrofuran), due to the absence of tyrosinate ions in the medium. Thus, we can predict that the reaction proceeds according to the path shown, and is confirmed through UV/Vis, fluorescence, and EPR spectroscopy and is discussed later in this section.

$$\text{tyrosine} \xrightarrow{\text{pH}>10} \text{tyrosinate} \xrightarrow{M^{n+}} \text{oxidized form of tyrosinate} + M$$

Sjodin et al. and Carra et al. reported that the oxidation of tyrosine proceeds through a pH-dependent electron transfer from tyrosine to a model compound, mimicking the photosystem II, containing ruthenium.[14,17] They have shown for pH values below the tyrosine pK_a ($pH < 10$), the tyrosine is initially protonated but at pH values above the tyrosine pK_a ($pH > 10$), the tyrosine is initially deprotonated. In both cases a single electron is transferred to the attached ruthenium complex. Thus, they have concluded that the mechanism is proton-coupled electron transfer at $pH < 10$, but is single-electron transfer at $pH > 10$ with a faster rate. On the basis of the above report and the characterization at each step of the GNP synthesis (our case) we have identified the chemistry in this reduction process. The fluorescence spectra of an aqueous solution of peptide-1 shows an emission peak at 348 nm ($E_{ex} = 275$ and 300 nm), corresponding to the tyrosinate form of the peptide at $pH > 10$ (Figure 4a and b) and shows an emission peak for both tyrosinate ($E_{em} = 348$ nm, $E_{ex} = 300$ nm) and tyrosine ($E_{em} = 321$ nm, $E_{ex} = 275$ nm) at $pH < 10$ as shown in Figure 4c and d respectively. Thus, the tyrosinate ion formed at both the above pH values (≈ 11 and 9) is responsible for the electron transfer to the nearby metal ion forming the metal nanoparticle and will be discussed in detail later in this section.

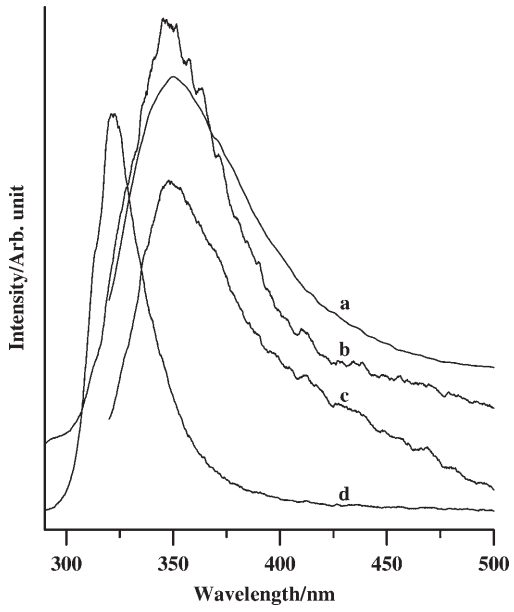

Figure 4. Emission spectra of neat peptide-1 at: a) $pH > 10$, excitation 275 nm; b) $pH > 10$, excitation 300 nm; c) $pH < 10$, excitation 300 nm; d) $pH < 10$, excitation 275 nm.

Fluorescence spectroscopic studies of tyrosine residues in peptide-1 also provided us with an indication of the modification of the tyrosine moiety during its reduction of Au^{III} to Au^{0}. In the presence of the gold salt, we observed the emission peak at about 410 nm upon excitation at 325 nm

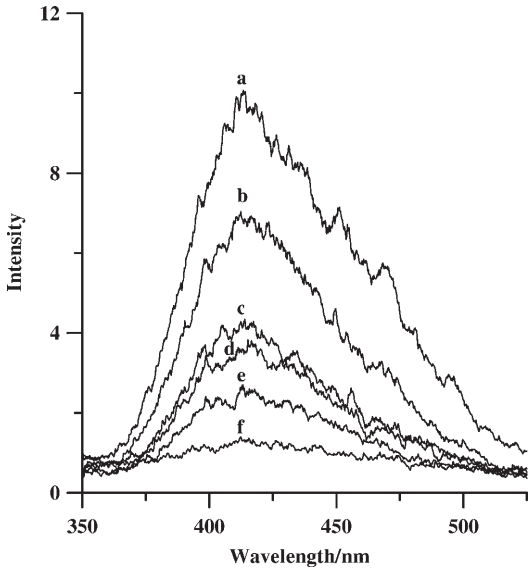

Figure 5. Emission spectra of gold-peptide-1 nanoconjugates during the progress of the reaction: a) 15 min; b) 30 min; c) 1.5 h; d) 5 h; e) 6.5 h; f) 3 days. The excitation wavelength is 325 nm at room temperature.

(Figure 5). The appearance of this peak may correspond to some modification in the tyrosine moiety of the peptide during the reduction process. There is very close structural similarity between tyrosine and *p*-cresol exhibiting similar UV/Vis and emission spectra. Odo et al. reported the oxidation of some *p*-hydroxyphenyl derivatives resulting in the formation of the dimeric fluorescent compounds, which emit in the same wavelength range as those in our case.[23] Thus the appearance of an emission peak at about 410 nm indicates the formation of the dityrosine form of peptide-1.[24–28]

For further confirmation, we studied the kinetics of GNP-formation by fluorescence spectroscopy ($E_{ex} = 325$ nm and $E_{em} = \sim 410$ nm). Figure 5 shows that the intensity of the dityrosine emission peak centered at about 410 nm decreased gradually as the reaction proceeded towards the end and finally there was no detectable peak. The decrease in emission intensity is due to quenching of the dityrosine fluorescence by the GNPs formed as mentioned in the literature.[29–31] The following experiments were carried out to provide more detailed evidence. The gold-peptide nanoconjugate formed was centrifuged, washed twice with triple-distilled water, redispersed in water, and the resulting suspension did not show any emission peak at 410 nm (Figure 6a).

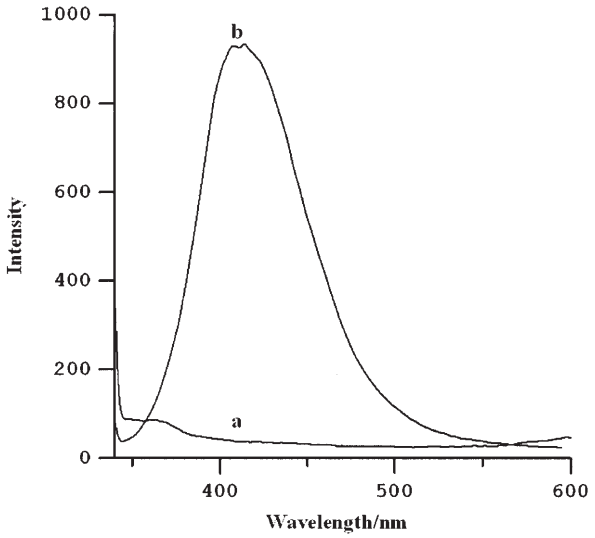

Figure 6. Emission spectra of centrifuged/washed and redispersed gold-peptide-1 nanoconjugates: a) before treatment with ethanolamine; b) after treatment with ethanolamine.

However, an emission peak was observed at about 410 nm ($E_{ex} = 325$ nm) on treatment with ethanolamine as shown in Figure 6b. We also observed a similar type of peak enhancement when tyrosine-reduced gold nanoparticles were treated with ethanolamine. (see Figure S3 in the Supporting Information). These observations indicate that the dityrosine part interacts with the GNP surface probably through its −OH group along with a free amino group of the peptides and hence their emission is quenched. When ethanolamine is added, it replaces the attached −OH group of the dityrosine form because of the stronger ligand, hence the −OH groups become free and there is an enhancement of peak intensity.

To provide further support for the emission peak position at around 410 nm, preformed citrate-stabilized GNPs were ligand-exchanged with the peptide-1 for 24 h at room temperature. The UV/Vis spectra of the resultant centrifuged/redispersed GNPs bound to peptide-1 did not show the absorbance peak corresponding to tyrosine/tyrosinate because of the very low concentration of surface-adsorbed peptide-1 molecules. However, the fluorescence spectra of these peptide-bound GNPs showed an emission peak at about 321 nm (see Figure S4 in the Supporting Information) characteristic of a tyrosine residue in peptide-1 as indicated in Figure 4d. This result indicates that there is no modification of tyrosine residues of peptide-1 during the ligand-exchange process. Thus, we can conclude that the tyrosine moiety converted to the dityrosine form in the presence of metal ions (in our case Au^{3+} and Ag^{+} ions) at basic pH and exhibited an emission peak at ~410 nm. A dityrosine bridge can only be formed when two tyrosyl radicals are linked together as depicted in Scheme 1, which proves that the reaction path goes through the radical mechanism.

The existence of intermediate tyrosyl radicals in the reduction of metal ion to metal by the transfer of an electron from the tyrosinate residue was also studied by EPR spectroscopy. We applied a microwave power of 10 mW and an amplitude modulation of 2×10 G. EPR spectra were recorded during the formation of GNPs by using peptide-1, but no sharp EPR signal for the tyrosyl radical was observed (Figure 7a). It has been reported in the literature that metal nanoparticles, more specifically the GNPs, quench the EPR signal of free radicals.[32–34] This might be the reason for the broadening of the EPR signal observed in the presence of GNPs. To investigate this, we recorded the EPR spectrum of a model system containing a Cu^{II} salt and peptide-1 in basic medium. The spectrum (Figure 7b), which was recorded immediately after the addition of the Cu^{II} salt to an alkaline peptide-1 solution, shows the EPR signal of the tyrosyl radical. The *g* value of the signal was found to be 1.9 close to the fingerprint *g* value for the tyrosyl radical.[35] The EPR signal attributed to the tyrosyl radical can be observed in

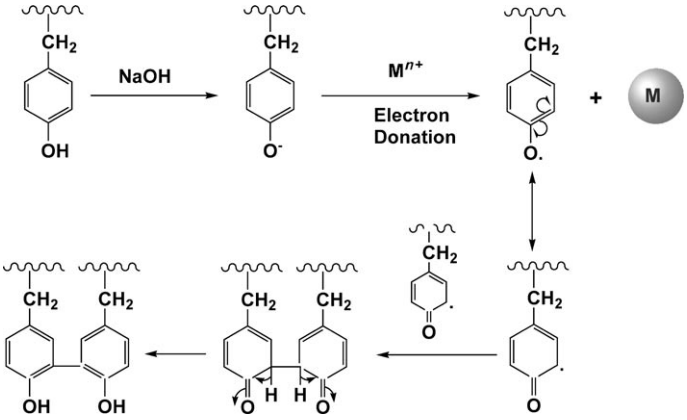

Scheme 1.

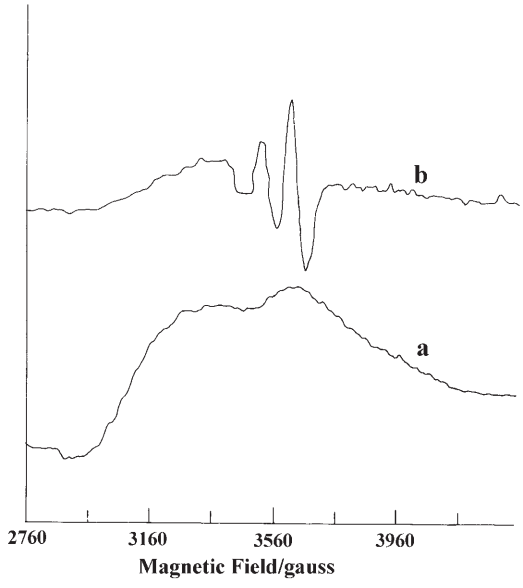

Figure 7. EPR spectra of peptide-1 after the addition of: a) $HAuCl_4$; and b) $Cu(NO_3)_2$ in basic medium. (The microwave power was 10 mW and amplitude modulation was 2×10 G).

the presence of peptide-1 because of the transfer of an electron from the tyrosinate ion to the Cu^{II} ion, which results in a conversion of Cu^{II} to Cu^{I} ions but not to metallic copper, due to a larger difference in the standard reduction potential. Since there is no metallic copper, there is no quenching of the EPR signal due to the interaction of the tyrosyl radical with the metal surface. Thus, we observed the EPR signal due to peptide-1 in the presence of a Cu^{II} salt in basic medium. (Figure 7b). However, the signal was not observed when the EPR measurement was taken some time after the addition of the peptides because of the formation of the dityrosine form of the peptide by the combination of two relatively long-lived tyrosyl radicals. The formation of dityrosine was further confirmed by taking the mass spectra of the extracted peptide-1 from the reaction medium that shows the presence of both the $[M^{+}+Na]$ and $[2M^{+}+Na]$ peak for the hydrolyzed peptide and its corresponding dimer respectively (see Figure S5 in the Supporting Information). We were unable to obtain mass spectra for the GNP-bound peptide-1 molecule because of problems in extracting the very small amount of adsorbed peptide molecules on the nanoparticle surface.

Thus during the process of the combination of two tyrosyl radicals to a stable and highly fluorescent dityrosine form, a proton is eliminated from each tyrosine of the dityrosine form of the peptide to retain its aromaticity (see Scheme 1). As a result, the pH of the reaction medium decreased from about 11 to 8–9 after completion of the reaction, because the released proton counterbalanced the hydroxide ion present in the medium. These results further substantiate that the formation of GNPs and the dityrosine by-product proceeds through the reaction mechanism as presented in Scheme 1.

To explore the fate of the tyrosine residue in the peptide after the reduction, the following experiments were performed. For this, as-prepared gold-peptide-1 nanoconjugate suspension was centrifuged (2.8×10^{4} g) for 1 h. The centrifuged nanoconjugates and the supernatant were then separately reacted with a freshly prepared $HAuCl_4$ solution at basic pH. In the first case, some new gold nanoparticles were formed as evident from the increase of the SP peak intensity after 24 h and 48 h of reaction, but after 72 h the intensity decreases due to aggregation (see Figure S6 in the Supporting Information). These particles were precipitated upon standing indicating that the GNPs were not stabilized due to less availability of peptide molecules in the reaction medium. Thus, we presumed that the dityrosine that was adsorbed on the nanoparticle surface might further reduce the metal ion present in solution. In the case of the supernatant, again a stable GNP suspension formed. Thus, we concluded that the reducing power of the tyrosine remains intact even after its conversion to the dityrosine form.

The rate of GNP formation by peptide-1 was studied from the increase in the SP band intensity of GNPs with time both at pH ~ 9 and ~11. This kinetic study showed that the rate of GNP formation is much faster at pH ~ 11 than at pH ~ 9 (compare Figure 8a and b). Thus, we can say that the electron transfer by the tyrosine residue is faster at pH ~ 11 than at pH ~ 9, which agrees well with data reported by Sjodin et al. and Carra et al.[14,17] When the reaction was performed at pH > 10, most of the tyrosine remained in the "tyrosinate" form as evident from the emission study discussed earlier (Figure 4). This form is more likely to undergo the electron transfer that causes the increase of the rate of GNP formation at pH ~ 11 compared to pH ~ 9. The rate of GNP formation, that is, the rate of electron donation, also depends on the availability of the number of tyrosinate species present in the reaction medium, which has been further confirmed by performing the reaction with peptide-2 and peptide-3 having two and three tyrosine residues, respectively. As the number of tyrosine residues was increased in the peptides, the effective donation of electrons increased to two- and three-fold respectively and thus we expected that the rate of GNP formation to also increase in the same fashion. To explore this in more detail, the formation of GNPs was monitored by the evaluation of the SP band during the nanoparticle formation (see Figure 8) by using peptides-1, -2, and -3. The spectral evolution is further analyzed in terms of the time dependence in the absorbance of the SP band. Figure 9 shows a plot of absorbance of the respective SP band due to these three peptides with respect to time. It clearly indicates that the rate of GNP formation increases almost linearly with time with a slight deviation in the case of peptide-3. The induction periods for GNP formation with peptides-1 and -2 are almost equal, but in the case of peptide-3 the induction time is slightly longer and may be due to the poor solubility of peptide-3 in the reaction medium. Once the GNP formation starts, the rate becomes faster compared to that of peptide-1 and peptide-2. From the slope, we observed that the rate of GNP formation using peptide-2 is exactly double that of peptide-1, as we expected. However, in the case of peptide-3, the rate of formation is three times that of peptide-1 only up to 70 min of reaction, as we expected, but after 70 min, the rate is little faster. We are unable to explain this observation at the moment.

Conclusion

Tyrosine-containing peptides were designed to synthesize colloidal gold and silver nanoparticles. A TEM study shows that the average particle size of gold nanoparticles increases with increasing number of peptide tyrosine residues, but the monodispersity of the particles increases. The reducing property of the tyrosine in the peptide depends on the pH of the medium. The formation of metal nanoparticles was followed by a radical mechanism producing the dityrosine form of the peptide through the tyrosyl radical intermediate, and was confirmed through UV/Vis, fluorescence, and EPR spectroscopy. Also the rate of reaction depends on the number of tyrosine moieties present in the peptide molecules. Finally, the dityrosine form of the peptide produced during the reaction is capable of reducing the gold salt to gold nanoparticles.

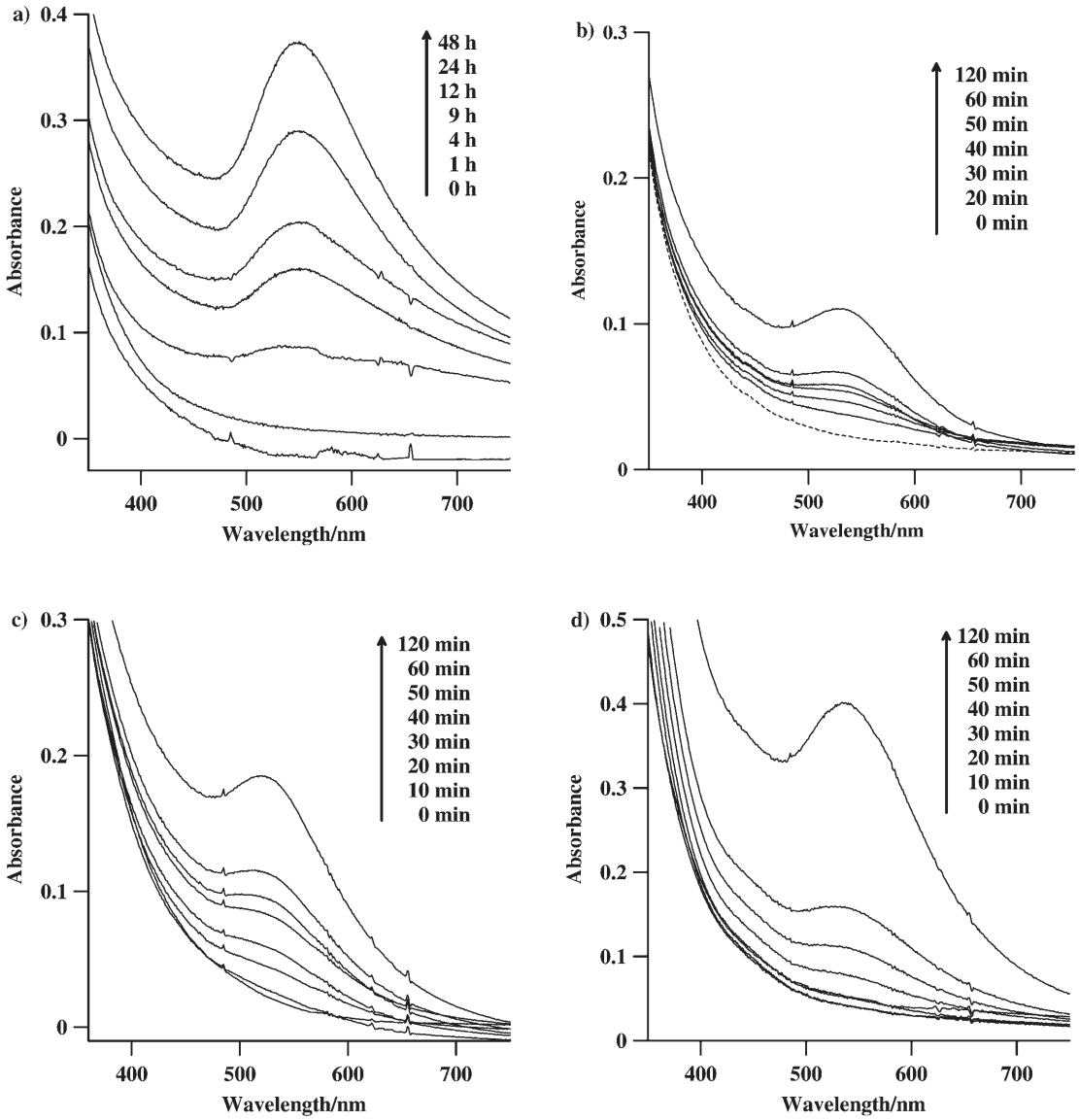

Figure 8. UV/Vis kinetic study of GNP formation with: a) peptide-1 at pH 9; b) peptide-1 at pH 11; c) peptide-2 at pH 11; and d) peptide-3 at pH 11.

Experimental Section

Materials: Dicyclohexylcarbodiimide (DCC), 1-hydroxybenzotriazole (HOBt), L-tyrosine (Tyr), α-aminoisobutyric acid (Aib), L-leucine (Leu), hydrogen tetrachloroaurate(III)trihydrate ($HAuCl_4 \cdot 3H_2O$), silver nitrate ($AgNO_3$), copper nitrate ($Cu(NO_3)_2 \cdot 3H_2O$), and ethanolamine were purchased from Sigma–Aldrich and were used as received. All the aqueous solutions were made with triple-distilled water. All other solvents were of analytical grade and used after distillation.

Synthesis of peptides: The tripeptides were synthesized by conventional solution-phase methods by using a racemization-free fragment-condensation strategy. The Boc group was used to protect the N-terminus and the C-terminus was protected as a methyl ester. Couplings were mediated by dicyclohexylcarbodiimide/1-hydroxybenzotriazole (DCC/HOBt). All intermediates have been characterized by ^{1}H NMR (300 MHz) and thin-layer chromatography (TLC) on silica gel and were used without further purification. The final products were purified by column chromatography using silica gel (100–200-mesh size) as the stationary phase and ethyl acetate/toluene as eluent. Purified final compounds have been fully characterized by 300 MHz ^{1}H NMR spectroscopy.

Synthesis of Boc-Tyr(1)-OH: A solution of Tyr (1.81 g, 10 mmol) in a mixture of dioxane (20 mL), water (10 mL), and 1 M NaOH (10 mL) was stirred and cooled in an ice/water bath. Di-*tert*-butylpyrocarbonate (2.4 g, 10 mmol) was then added to the above mixture and stirred for 6 h at 25 °C. The solution was concentrated in vacuum (10–20 mL), cooled in an ice/water bath, covered with a layer of ethyl acetate (about 15 mL), and acidified with a dilute solution of $KHSO_4$ to obtain a solution of pH 2–3. The aqueous phase containing the peptides was extracted with ethyl acetate (3×30 mL), was dried over anhydrous Na_2SO_4, and was evaporated in vacuum. The pure material was obtained as a waxy solid. Yield = 2.67 g (9.5 mmol, 95 %).

Synthesis of Boc-Tyr(1)-Aib(2)-OMe: A sample of Boc-Tyr-OH (2.53 g, 9 mmol) was dissolved in dichloromethane (DCM) (20 mL) in an ice/water bath. H-Aib-OMe was isolated from the corresponding methyl ester hydrochloride (4.17 g, 18 mmol) by neutralization and subsequent extraction with ethyl acetate and the extract was concentrated to 5 mL. This was added to the reaction mixture, followed immediately by dicyclo-

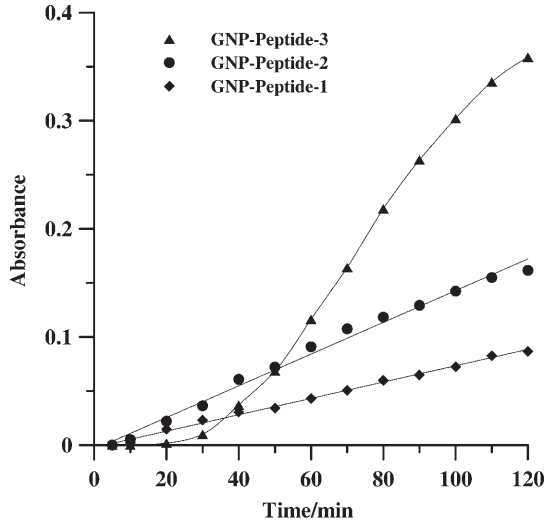

Figure 9. Plots of absorbance against time for the respective surface plasmon bands of GNPs prepared using peptides-1, -2, and -3 at pH 11.

hexylcarbodiimide (DCC) (1.854 g, 9 mmol). The reaction mixture was allowed to come to room temperature and was stirred for 24 h. DCM was evaporated, and the residue was taken up in ethyl acetate (30 mL), and dicyclohexylurea (DCU) was filtered off. The organic layer was washed with HCl (2 M, 3×30 mL), brine (30 mL), sodium carbonate (1 M, 3×30 mL), and brine (2×30 mL), and was dried over anhydrous sodium sulfate, followed by evaporation in vacuum to yield a white solid. Yield = 3 g (7.91 mmol, 87.8 %); ^{1}H NMR (300 MHz, $CDCl_3$, TMS): δ = 7.1–7.08 (d, J = 8.4 Hz, 2H; Tyr(1) ring hydrogen), 6.78–6.75 (d, J = 8.5 Hz, 2H; Tyr(1) ring hydrogen), 6.29 (s, 1H; Aib(2) N–H), 5.37 (d, J = 6.5 Hz, 1H; Tyr(1) N–H), 4.15–4.68 (m, 1H; Tyr(1) C$^\alpha$H), 3.79 (s, 3H; OCH_3), 3.1–2.8 (m, 2H; Tyr(1) C$^\beta$H), 1.55 (s, 6H; Aib(2) C$^\beta$H), 1.42 ppm (s, 9H; Boc-CH_3).

Synthesis of Boc-Tyr(1)-Aib(2)-OH: MeOH (30 mL) and NaOH (2 M, 10 mL) were added to a sample of Boc-Tyr(1)-Aib(2)-OMe (3 g, 7.9 mmol), and the progress of saponification was monitored by thin-layer chromatography (TLC). The reaction mixture was stirred for 10 h. Then methanol was removed under vacuum, the residue was taken up in 30 mL of water and was washed with diethyl ether (2×20 mL). Then the pH of the aqueous layer was adjusted to 2 using HCl (1 M) and was extracted with ethyl acetate (3×20 mL), dried over anhydrous sodium sulfate, and evaporated in vacuum to yield a white solid. Yield = 2.74 g (7.5 mmol, 95 %).

Synthesis of Boc-Tyr(1)-Aib(2)-Tyr(3)-OMe: A sample of Boc-Tyr(1)-Aib(2)-OH (2.7 g, 7.5 mmol) in DMF (8 mL) was cooled in an ice/water bath and H-Tyr-OMe was isolated from the corresponding methyl ester hydrochloride (4.2 g, 15 mmol) by neutralization, subsequent extraction with ethyl acetate and concentration (5 mL), and was added to the reaction mixture followed immediately by DCC (1.5 g, 7.5 mmol) and HOBt (1 g, 7.5 mmol). The reaction mixture was stirred for 3 days. The residue was taken up in ethyl acetate (20 mL) and the DCU was filtered off. The organic layer was washed with HCl (2 M, 3×20 mL), brine (30 mL), sodium carbonate (1 M, 3×20 mL), brine (2×20 mL), dried over anhydrous sodium sulfate and evaporated in vacuum to yield a white solid. Purification was performed by silica gel column (100–200 mesh) using ethyl acetate/toluene (2:1) as eluent. Yield = 3.26 g (6 mmol, 80 %); ^{1}H NMR (300 MHz, $CDCl_3$ + 5 % DMSO, TMS): δ = 7.01–6.98 (d, J = 8.4 Hz, 2H; Tyr(1)/Tyr(3) ring hydrogen), 6.93–6.90 (d, J = 8.4 Hz, 2H; Tyr(1)/Tyr(3) ring hydrogen), 6.83 (d, J = 6.33 Hz, 1H; Tyr(3) N–H), 6.77–6.74 (d, J = 8.4 Hz, 2H; Tyr(1)/Tyr(3) ring hydrogen), 6.75–6.72 (d, J = 8.4 Hz, 2H; Tyr(1)/Tyr(3) ring hydrogen), 6.31 (s, 1H; Aib(2) N–H), 5.32 (d, J = 6.5, 1H; Tyr(1) N–H), 4.77–4.70 (m, 1H; Tyr(1) C$^\alpha$H), 4.1–4.15 (m, 1H; Tyr(3) C$^\alpha$H), 3.7 (s, 3H; OCH_3), 3.1–2.81 (m, 4H; Tyr(1) & Tyr(3) C$^\beta$H), 1.41 (s, 9H; Boc-CH_3), 1.35 ppm (d, J = 12.9, 6H; Aib(2) C$^\beta$H); elemental analysis calcd (%) for $C_{28}H_{37}N_3O_8$ (543): C 61.88, H 6.81, N 7.73; found: C 61.51, H 6.47, N 7.43; MS (ESI) (35 eV): m/z (%): 566 (100) [M^++Na].

Synthesis of peptide-2, (NH_2-Tyr(1)-Aib(1)-Tyr(3)-OMe): We added formic acid (10 mL, 98 %) to Boc-Tyr(1)-Aib(2)-Tyr(3)-OMe (5 mM) and the removal of the Boc-group was monitored by TLC. After 8 h, the formic acid was removed under vacuum. The residue was taken up in water (20 mL) and was washed with diethyl ether (2×20 mL). The pH of the aqueous solution was then adjusted to 8 with sodium bicarbonate and the solution was extracted with ethyl acetate (3×30 mL). The organic extract was washed with saturated brine, dried over sodium sulfate, and was concentrated to a viscous liquid that gave a positive ninhydrin test. ^{1}H NMR (300 MHz, $CDCl_3$ + 5 % DMSO, TMS): δ = 8.45 (br, 2H; Tyr(1) NH_2), 7.63 (s, 1H; Aib(2) N–H), 7.27–7.25 (d, J = 7.5 Hz, 1H; Tyr(3) N–H), 7.04–7.01 (d, J = 8.4 Hz, 2H; Tyr(1)/Tyr(3) ring hydrogen), 6.96–93 (d, J = 8.4 Hz, 2H; Tyr(1)/Tyr(3) ring hydrogen), 6.8–6.77 (d, J = 8.4 Hz, 2H; Tyr(1)/Tyr(3) ring hydrogen), 6.76–6.73 (d, J = 8.4 Hz, 2H, Tyr(1)/Tyr(3) ring hydrogen), 4.76–4.69 (m, 1H; Tyr(3) C$^\alpha$H), 4.13–4.1 (m, 1H; Tyr(1) C$^\alpha$H), 3.7 (s, 3H; OCH_3), 3.11–2.94 (m, 4H; Tyr(1) & Tyr(3) C$^\beta$H), 1.48 ppm (d, J = 8.55 Hz, 6H; Aib(2) C$^\beta$H); elemental analysis calcd (%) for $C_{23}H_{29}N_3O_6$ (443): C 62.30, H 6.54, N 9.48; found: C 62.36, H 6.58, N 9.38; MS (ESI) (35 eV): m/z (%): 466 (100) [M^++Na].

Synthesis of Boc-Tyr(1)-Tyr(2)-OMe: A sample of Boc-Tyr-OH (2.53 g, 9 mmol) was dissolved in dichloromethane (DCM) (20 mL) in an ice/water bath. H-Tyr-OMe was isolated from the corresponding methyl ester hydrochloride (4.17 g, 18 mmol) by neutralization and subsequent extraction with ethyl acetate, and was concentrated to 5 mL. This was added to the reaction mixture, followed immediately by dicyclohexylcarbodiimide (DCC) (1.854 g, 9 mmol). The reaction mixture was allowed to come to room temperature and was stirred for 24 h. The DCM was evaporated, and the residue was taken up in ethyl acetate (30 mL), and dicyclohexylurea (DCU) was filtered off. The organic layer was washed with HCl (2 M, 3×30 mL), brine (30 mL), sodium carbonate (1 M, 3×30 mL), and brine (2×30 mL), and was dried over anhydrous sodium sulfate, followed by evaporation in vacuum to yield a white solid. Yield = 3.66 g (8 mmol, 88.8 %); ^{1}H NMR (300 MHz, $CDCl_3$, TMS): δ = 7.03–7.00 (d, J = 8.4 Hz, 2H; Tyr(1)/Tyr(2) ring hydrogen), 6.83–6.80 (d, J = 8.4 Hz, 2H; Tyr(1)/Tyr(2) ring hydrogen), 6.71–6.68 (d, J = 8.34 Hz, 2H; Tyr(1)/Tyr(2) ring hydrogen), 6.70–6.67 (d, J = 8.4 Hz, 2H; Tyr(1)/Tyr(2) ring hydrogen), 6.1 (d, J = 6.2 Hz, 1H; Tyr(2) N–H), 5.03 (d, J = 6.0 Hz, 1H; Tyr(1) N–H), 4.74–4.71 (m, 1H; Tyr(2) C$^\alpha$H), 4.15–4.08 (m, 1H; Tyr(1) C$^\alpha$H), 3.69 (s, 3H; OCH_3), 3.02–2.85 (m, 4H; Tyr(1) & Tyr(2) C$^\beta$H), 1.42 ppm (s, 9H; Boc-CH_3).

Synthesis of Boc-Tyr(1)-Tyr(2)-OH: We added MeOH (30 mL) and NaOH (10 mL, 2 M) to a sample of Boc-Tyr(1)-Tyr(2)-OMe (3.66 g, 8 mmol), and the progress of saponification was monitored by TLC. The reaction mixture was stirred. After 10 h, methanol was removed under vacuum, the residue was taken up in 30 mL of water, and was washed with diethyl ether (2×20 mL). The pH of the aqueous layer was adjusted to 2 using HCl (1 M) and was then extracted with ethyl acetate (3×20 mL), was dried over anhydrous sodium sulfate, and was evaporated in vacuum to yield a white solid. Yield = 3.3 g (7.5 mmol, 93.7 %).

Synthesis of Boc-Tyr(1)-Tyr(2)-Tyr(3)-OMe: A sample of Boc-Tyr(1)-Tyr(2)-OH (3.3 g, 7.5 mmol) in DMF (8 mL) was cooled in an ice/water bath and H-Tyr-OMe was isolated from the corresponding methyl ester hydrochloride (3.46 g, 15 mmol) by neutralization, subsequent extraction with ethyl acetate and concentration (5 mL), and was added to the reaction mixture followed immediately by DCC (1.54 g, 7.5 mmol) and HOBt (1.01 g, 7.5 mmol). The reaction mixture was stirred for three days. The residue was taken up in ethyl acetate (20 mL) and the DCU was filtered off. The organic layer was washed with HCl (2 M, 3×20 mL), brine (30 mL), sodium carbonate (1 M, 3×20 mL), brine (2×20 mL), and was dried over anhydrous sodium sulfate, followed by evaporation in vacuum to yield a white solid. Purification was performed with a silica gel column (100–200 mesh) using ethyl acetate/toluene (2:1) as eluent. Yield = 5.3 g (8.5 mmol, 85.3 %); ^{1}H NMR (300 MHz, $CDCl_3$ + 5 % DMSO, TMS): δ = 6.94–6.92 (d, J = 8.4 Hz, 2H; Tyr(1)/Tyr(2)/Tyr(3) ring hydrogen),

6.88–6.85 (d, $J=8.3$ Hz, 2H; Tyr(1)/Tyr(2)/Tyr(3) ring hydrogen), 6.84–6.81 (d, $J=8.4$ Hz, 2H; Tyr(1)/Tyr(2)/Tyr(3) ring hydrogen), 6.74–6.71 (d, $J=8.4$ Hz, 2H; Tyr(1)/Tyr(2)/Tyr(3) ring hydrogen), 6.71–6.68 (d, $J=8.4$ Hz, 2H; Tyr(1)/Tyr(2)/Tyr(3) ring hydrogen), 6.50–6.48 (d, $J=6.2$ Hz, 1H; Tyr(1)/Tyr(2)/Tyr(3) N−H), 6.41–6.39 (d, $J=7.5$ Hz, 1H; Tyr(1)/Tyr(2)/Tyr(3) N−H), 5.09–5.06 (d, $J=7.62$ Hz, 1H; Tyr(1)/Tyr(2)/Tyr(3) N−H), 4.68–4.61 (m, 1H; Tyr(1)/Tyr(2)/Tyr(3) $C^{\alpha}H$), 4.50–4.43 (m, 1H; Tyr(1)/Tyr(2)/Tyr(3) $C^{\alpha}H$), 4.24–4.22 (m, 1H; Tyr(1)/Tyr(2)/Tyr(3) $C^{\alpha}H$), 3.68 (s, 3H; OCH_3), 3.02–2.78 (m, 6H; Tyr(1)+Tyr(2)+Tyr(3) $C^{\beta}H$), 1.39 ppm (s, 9H; Boc-CH_3); elemental analysis calcd (%) for $C_{33}H_{39}N_3O_9$ (621): C 63.77, H 6.28, N 6.76; found: C 63.21, H 6.29, N 6.13; MS (ESI) (35 eV): *m/z* (%): 644 (100) [M^++Na].

Synthesis of peptide-3, (NH_2-Tyr(1)-Tyr(2)-Tyr(3)-OMe): We added formic acid (10 mL, 98%) to 5 mM of Boc-Tyr(1)-Tyr(2)-Tyr(3)-OMe and the removal of the Boc-group was monitored by TLC. After, 8 h, the formic acid was removed under vacuum. The residue was taken up in water (20 mL), and was washed with diethyl ether (2×20 mL). The pH of the aqueous solution was then adjusted to 8 with sodium bicarbonate and the solution was then extracted with ethyl acetate (3×30 mL). The organic extract was washed with saturated brine, dried over sodium sulfate, and was concentrated to a viscous liquid that gave a positive ninhydrin test. ^{1}H NMR (300 MHz, $CDCl_3$ + 5% DMSO, TMS): $\delta=8.41$ (br, 2H; Tyr(1) NH_2), 7.7–7.68 (d, $J=8.4$ Hz, 1H; Tyr(2)/Tyr(3) N−H), 7.00–6.65 (m, 12H; Tyr(1)+Tyr(2)+Tyr(3) ring hydrogen), 4.73–4.66 (m, 1H; Tyr(1)/Tyr(2)/Tyr(3) $C^{\alpha}H$), 4.59–4.52 (m, 1H; Tyr(1)/Tyr(2)/Tyr(3) $C^{\alpha}H$), 4.24–4.21 (m, 1H; Tyr(1)/Tyr(2)/Tyr(3) $C^{\alpha}H$), 3.68 (s, 3H; OCH_3), 3.02–2.85 ppm (m, 6H; Tyr(1)+Tyr(2)+Tyr(3) $C^{\beta}H$); elemental analysis calcd (%) for $C_{28}H_{31}N_3O_7$ (521): C 64.49, H 5.95, N 8.06; found: C 64.13, H 6.43, N 7.89; MS (ESI) (35 eV): *m/z* (%): 544 (100) [M^++Na].

Synthesis of metal–peptide nanoconjugates: The detailed synthesis of gold-peptide-1 nanoconjugates has been described in our earlier report.[11] Similarly, 40 mM of a solution of peptide-2 and peptide-3 (in methanol) was added to an aqueous solution of $HAuCl_4$ (10 mM), such that the final concentration of respective peptide and $HAuCl_4$ was 5 mM and 2.5 mM respectively. In both the reactions the desired pH values were maintained using standard NaOH solution.

Characterization

NMR experiments: All NMR studies were carried out on a Bruker DPX 300 MHz spectrometer. Peptide concentrations were in the range 1–10 mM in $CDCl_3$ and DMSO.

GNP formation by UV/Vis spectrophotometry: UV/Vis absorption spectra of all the nanoconjugate suspensions were measured in a Hewlett–Packard 8453 spectrophotometer. For the kinetic study, the UV/Vis spectra were recorded from time-to-time during the reaction with samples in a 0.1 cm quartz cuvette. The rate of formation of GNPs was monitored by the time-dependent evaluation of the SP band of the gold nanoparticles.

Fluorescence spectroscopy: Emission spectra of peptides/nanoconjugates were recorded on a Perkin–Elmer LS55 fluorimeter. The emission spectra of gold-peptide-1 nanoconjugates were also recorded occasionally during their formation by conducting the reaction in a 1 cm quartz cell and by using an excitation wavelength of 325 nm.

EPR study: Formation of intermediate tyrosyl radicals during the reaction of an alkaline solution of the peptide-1 and $HAuCl_4$ or $Cu(NO_3)_2$ was monitored by recording the instantaneous EPR spectra of the above-mixture using a Varian E-112 spectrometer.

Mass spectral study: First, an alkaline solution of the peptide-1 was treated with $Cu(NO_3)_2$. The product of this reaction, that is supposed to be a mixture of unreacted peptide-1 and the dityrosine form of the peptide, was then extracted back from the reaction solution and used for ESI mass analysis in a quadrupole time-of-flight (Qtof) Micro YA263 mass spectrometer.

Acknowledgements

S.S. thanks the CSIR, Government of India for providing a Senior Research Fellowship. This research was supported by grants [Grant No. BT/PR3648/BRB/10/301/2003] from the Department of Biotechnology, New Delhi. Thanks are also due to the partial support from the Nanoscience and Nanotechnology Initiatives, DST, New Delhi. We also thank the SAIF, Bose Institute, Kolkata for recording the EPR spectra.

[1] U. Kreibig, M. Vollmer in *Optical Properties of Metal Clusters*, Springer Series in Materials Science, No. 25, Springer, Berlin, **1995**.
[2] J. R. Krenn, B. Lamprecht, H. Ditlbacher, G. Schider, M. Salerno, A. Leitner, F. R. Aussenegg, *Europhys. Lett.* **2002**, *60*, 663–669.
[3] J. J. Storhoff, R. Elghanian, R. C. Mucic, C. A. Mirkin, R. L. Letsinger, *J. Am. Chem. Soc.* **1998**, *120*, 1959–1964.
[4] A. Gole, C. Dash, V. Ramakrishnan, S. R. Sainkar, A. B. Mandale, M. Rao, M. Sastry, *Langmuir* **2001**, *17*, 1674–1679.
[5] A. P. Alivastos, K. P. Johnson, X. Peng, T. E. Wilson, C. J. Loweth, M. P. Bruchez, P. G. Schultz, *Nature* **1996**, *382*, 609–611.
[6] S. Mann, W. Shenton, M. Li, S. Connolly, D. Fitzmaurice, *Adv. Mater.* **2000**, *12*, 147–150.
[7] C. A. Mirkin, R. L. Letsinger, R. C. Mucic, J. J. Storhoff, *Nature* **1996**, *382*, 607–609.
[8] W. Shenton, S. A. Davis, S. Mann, *Adv. Mater.* **1999**, *11*, 449–452.
[9] Y. Zhou, W. Chen, H. Itoh, K. Naka, Q. Ni, H. Yamane, Y. Chujo, *Chem. Commun.* **2001**, 2518–2519.
[10] P. R. Selvakannan, A. Swami, D. Srisathiyanarayanan, P. S. Shirude, R. Pasricha, A. B. Mandale, M. Sastry, *Langmuir* **2004**, *20*, 7825–7836.
[11] R. R. Bhattacharjee, A. K. Das, D. Haldar, S. Si, A. Banerjee, T. K. Mandal, *J. Nanosci. Nanotechnol.* **2005**, *5*, 1141–1147.
[12] B. A. Barry, M. K. El-Deeb, P. O. Sandusky, G. T. Babcock, *J. Biol. Chem.* **1990**, *265*, 20139–20143.
[13] S. Kim, J. Liang, B. A. Barry, *Proc. Natl. Acad. Sci. USA* **1997**, *94*, 14406–14411.
[14] M. Sjodin, S. Styring, B. Åkermark, L. Sun, L. Hammarstrom, *J. Am. Chem. Soc.* **2000**, *122*, 3932–3936.
[15] W. Hofbauer, A. Zouni, R. Bittl, J. Kern, P. Orth, F. Lendzian, P. Fromme, H. T. Witt, W. Lubitz, *Proc. Natl. Acad. Sci. USA* **2001**, *98*, 6623–6628.
[16] R. Ghanem, Y. Xu, J. Pan, T. Hoffmann, J. Andersson, T. Polivka, T. Pascher, S. Styring, L. Sun, V. Sundstrom, *Inorg. Chem.* **2002**, *41*, 6258–6266.
[17] C. Carra, N. Iordanova, S. Hammes-Schiffer, *J. Am. Chem. Soc.* **2003**, *125*, 10429–10436.
[18] L. W. Smith, T. E. Eling, R. J. Kulmacz, L. J. Marnett, A.-L. Tsai, *Biochemistry* **1992**, *31*, 3–7.
[19] M. M. Whittaker, J. W. Whittaker, *J. Biol. Chem.* **1990**, *265*, 9610–9613.
[20] A. Larsson, B.-M. Sjoberg, *EMBO J.* **1986**, *5*, 2037–2040.
[21] J. A. Creighton, D. G. Eadon, *J. Chem. Soc. Faraday Trans.* **1991**, *87*, 3881–3891.
[22] R. Levy, N. T. K. Thanh, R. C. Doty, I. Hussain, R. J. Nichols, D. J. Schiffrin, M. Brust, D. G. Fernig, *J. Am. Chem. Soc.* **2004**, *126*, 10076–10084.
[23] J. Odo, K. Matsumoto, E. Shinmoto, Y. Hatae, A. I. Shiozaki, *Anal. Sci.* **2004**, *20*, 707–710.
[24] T. G. Huggins, M. C. Wells-Knecht, N. A. Detorie, J. W. Baynes, S. R. Thorpe, *J. Biol. Chem.* **1993**, *268*, 12341–12347.
[25] E. Assemand, M. Lacroix, M. A. Mateescu, *Biotechnol. Appl. Biochem.* **2003**, *38*, 151–156.
[26] K. J. A. Davies, *J. Biol. Chem.* **1987**, *262*, 9895–9901.
[27] J. S. Jacob, D. P. Cistola, F. F. Hsu, S. Muzaffar, D. M. Mueller, S. L. Hazen, J. W. Heinecke, *J. Biol. Chem.* **1996**, *271*, 19950–19956.
[28] D. A. Malencik, J. F. Sprouse, C. A. Swanson, S. R. Anderson, *Anal. Biochem.* **1996**, *242*, 202–213.
[29] I. Pockrand, A. Brillante, D. Mobius, *Chem. Phys. Lett.* **1980**, *69*, 499–504.

[30] A. C. Pineda, D. Ronis, *J. Chem. Phys.* **1985**, *83*, 5330–5337.
[31] D. J. Maxwell, J. R. Taylor, S. Nie, *J. Am. Chem. Soc.* **2002**, *124*, 9606–9612.
[32] D. Kivelson, *J. Chem. Phys.* **1960**, *33*, 1094–1106.
[33] P. Ionita, A. Caragheorgheopol, B. C. Gilbert, V. Chechik, *J. Am. Chem. Soc.* **2002**, *124*, 9048–9049.
[34] Z. Zhang, A. Berg, H. Levanon, R. W. Fessenden, D. Meisel, *J. Am. Chem. Soc.* **2003**, *125*, 7959–7963.
[35] I. Ayala, K. Range, D. York, B. A. Barry, *J. Am. Chem. Soc.* **2002**, *124*, 5496–5505.

Received: July 18, 2005
Published online: November 9, 2005

